

A Benchtop Flight Control Demonstrator

Joris R. Duran James F. Whidborne* Martin Carrizales Rodriguez
Alessandro Pontillo

April 2019

Abstract

A feedback control demonstrator is described. The demonstrator is intended for the demonstration of control principles applied to flight control of fixed-wing aircraft and hence is suitable for aeronautical programmes. The demonstrator consists of a two degree-of-freedom wing assembly where the wing is free to pitch in an airflow provided by a simple, benchtop wind tunnel. The second degree-of-freedom is provided by a hinged elevator which is actuated by a servomotor. The wing pitch angle is measured with a potentiometer attached to a pivot shaft, thus allowing feedback control of the elevator pitch to be implemented. The aerodynamics of the wing are modelled, the wind tunnel design is described and computational fluid dynamics analysis presented. An embedded controller that implements a Proportional–Integral–Derivative (PID) controller and a graphical interface have been developed. Some details of these are also given.

Keywords: Laboratory Demonstrator, Flight Control, PID Control, Wind Tunnel, Aerospace Education

1 Introduction

Feedback control is ubiquitous in aircraft systems, and understanding the concept is essential for avionics engineers, flight dynamicists, flight test engineers and pilots, system engineers as well as, of course, flight control specialists. However, the concept of feedback is quite abstract, consequently many undergraduate learners struggle with first control courses, particularly in relating the abstract notions to physical systems. This has been identified as a ‘gap’ between the theory and practice [1] in that the controller must be controlling something physical, but the concepts of feedback and stability are abstract concepts expressed mathematically. To be able to see a feedback system in operation clearly helps students to visualize the concept as well as appreciate the utility of feedback.

Control educators have developed many laboratory-based examples of control systems over the years. These are usually process control oriented [2] or mechanical/mechatronics based [3]. However there are several laboratory based experiments on the market that are more appropriate for aerospace engineers. The well-known inverted pendulum has dynamics that make the stabilization problem similar to rocket or missile stabilization [4]. However the experiment does not use any aerodynamic forces and, to an inexperienced engineer, the relationship to aerospace problems is not obvious. There are a number of experiments that use aerodynamic controls. A simple propeller-based beam-levelling experiment is available, [5] and appears to be a good introduction. This idea has been extended to 2- and 3-DOF helicopter rigs [6, 7, 8]. A 3-DOF quadrotor-based rig is also available [9] from QUANSER. In fact QUANSER market a full flying lab suitable for indoor experiments [10]. All these kits are all useful and well-tested, but for first course experiments the beam-levelling experiment is most straightforward, being a single input system with simple dynamics. All the described equipment are based on rotorcraft technologies and there does not appear to be a fixed-wing based control experiment on the market. The closest is the Flight Demonstration Wind Tunnel from Tecquipment Academia [11]. This appears to be an excellent tool for flight dynamics demonstration, but has an open-loop control system driven by pilot-type controls, subsequently it does not illustrate feedback principles.

Hence to demonstrate the concept of feedback for students with a familiarity with the aerodynamics and flight dynamics of fixed-wing aircraft, a low-cost benchtop flight control demonstrator has been designed. In

*Centre for Aeronautics, Cranfield University, Bedfordshire MK45 0AL, UK. email:j.f.whidborne@cranfield.ac.uk

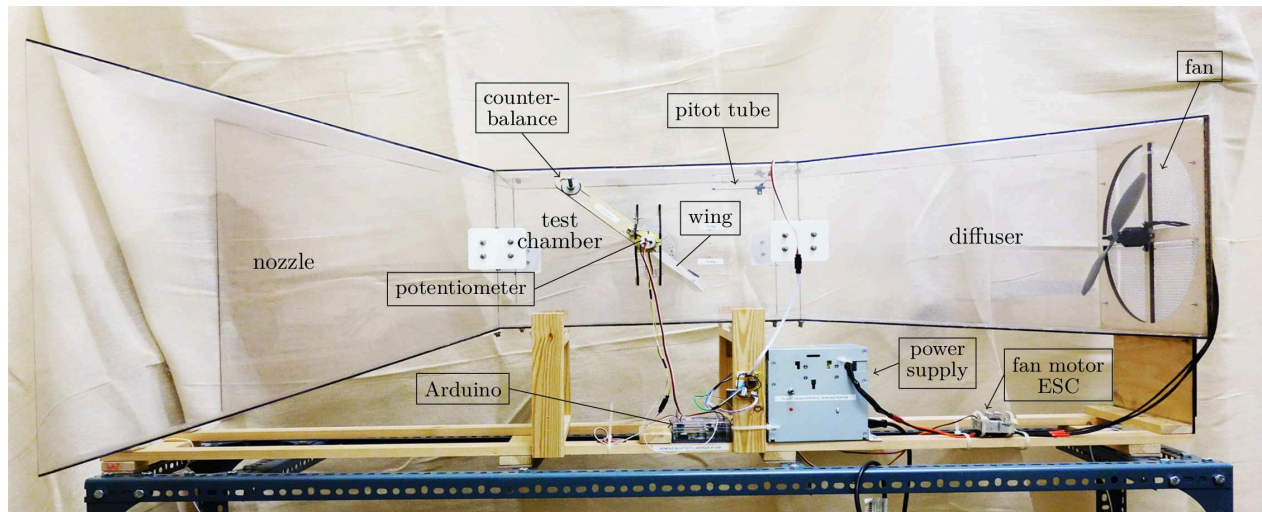


Figure 1: Benchtop flight control demonstrator.

in this paper the principles and design are described. The demonstrator is shown in Figure 1. The equipment consists of a small wind tunnel; in the test chamber there is a wing that can freely rotate about an axis and that includes a trailing edge control surface (elevator) that is actuated by a small servomotor. The wing pitch angle is measured using a potentiometer, and the signal is fed back to the servomotor via an Arduino microcontroller board that enacts a PID control algorithm. The control objective is to maintain the wing at a constant pitch angle that is defined from a Graphical User Interface (GUI) program running on a laptop PC. A schematic is shown in Figure 2.

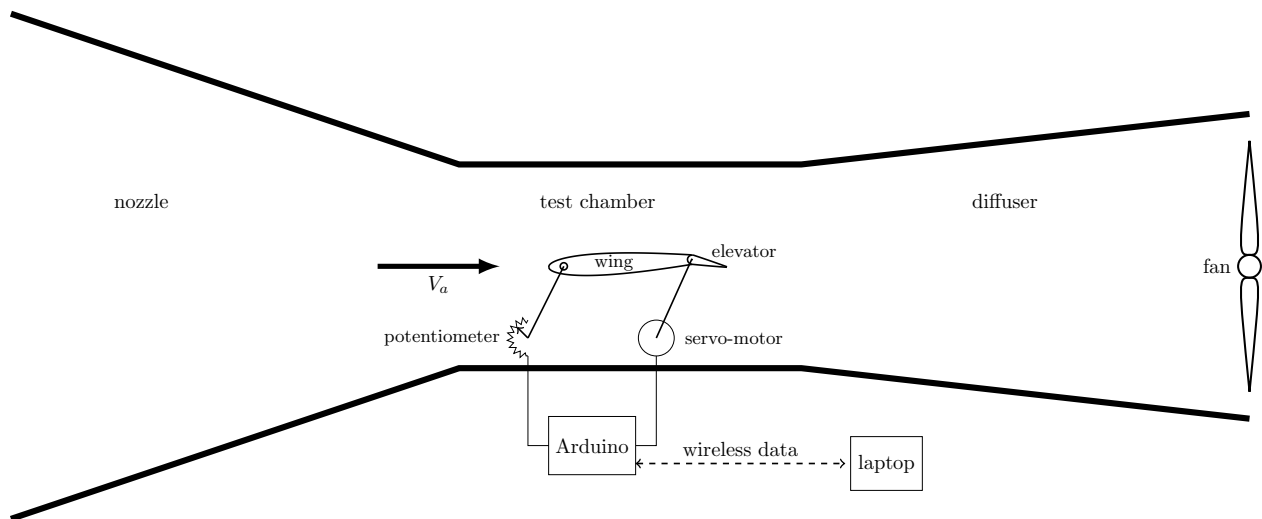


Figure 2: Equipment schematic.

The next section contains a description of the detail of the wind tunnel design along with Computational Fluid Dynamics (CFD) results describing the flow that validate the design. The wing aerofoil is then analyzed, and the wing design and construction are described. The next section briefly describes the electronics, microcontroller program and Graphical User Interface (GUI) respectively. Some controller parameter tuning and experimental results are described in the penultimate section before a concluding section.

Nomenclature

- α Angle of attack/pitch angle
- δ Elevator deflection angle
- ℓ_0 Length between aerodynamic centre and pivot point
- ν Kinematic viscosity for atmosphere at sea level
- ω_n Natural frequency of the model dominant mode
- ρ Air density
- τ Trailing edge angle
- τ_a Trailing edge parameter
- ε_1 Chord fraction location of wing pivot
- ε_2 Chord fraction location of control surface pivot from trailing edge
- ζ Damping ratio of the model dominant mode
- a Test chamber section width
- a_{1i} Inviscid lift-curve slope
- a_{1v} Viscous lift-curve slope of aerofoil
- a_{2T} Inviscid lift-curve slope with respect to control surface deflection
- a_{2v} Lift-curve slope with respect to control surface deflection
- b Friction and aerodynamic damping coefficient
- c Aerofoil chord length
- C_l Aerodynamic lift coefficient
- F_1 Ordinate in Figure 1 of ESDU 72024 [12]
- F_3 Ordinate in Figure 4 of ESDU 72024 [12]
- $G(s)$ Generic model Laplace transfer function
- I Wing moment of inertia
- k_g Generic model steady state gain
- k_p, k_i, k_d PID controller gains
- m_0 Moment-curve slope with respect to control surface deflection
- m_{0T} Inviscid flow moment-curve slope with respect to control surface deflection
- q Dynamic pressure, $q = 1/2\rho V_a^2$
- R_N Reynolds number
- S Wing area
- t Maximum thickness chord fraction
- $t_{0.99}$ Aerofoil profile thickness at $x = 0.99c$
- $t_{0.9}$ Aerofoil profile thickness at $x = 0.9c$
- V_a Nominal air flow speed
- x Distance from leading edge
- x_t Chordwise position of maximum thickness
- x_{ai} Aerodynamic centre
- z_t Half-thickness of the profile
- z_{t1} Profile half-thickness at $x = 0.005c$
- z_{t2} Profile half-thickness at $x = 0.05c$

2 Wind tunnel design

The purpose of the demonstrator is not to investigate the aerodynamic behaviour of the aerofoil, but to demonstrate the actions of a PID correction. Hence the wind tunnel is not designed to optimize the quality of the flow, but to provide a flow that can maintain the lift on the wing without disturbing it excessively and so making observation of the control operation difficult. Furthermore, the aim is to have a benchtop demonstrator than can be transported easily so that the demonstrator can be used during class. The equipment is straightforward to construct and, with the aid of a 3-D printer, the parts are not expensive. An outline of the design is given below, it mostly follows the guidelines given by Mauro *et al* [13].

The wind tunnel is divided into three parts: the nozzle, the test chamber and the diffuser as shown in Figure 2. Each part is connected to the other by four joint parts as seen in Figure 1. The wind tunnel is designed with simple shapes to make construction straightforward. The panels from the nozzle, the test chamber and the diffuser are cut out from 3mm transparent polycarbonate sheets using the laser-cut machine. The panels of each section of the wind tunnel are then glued together. The joint parts are 3D printed and make the gluing process easier. They are 5mm thick and screwed to the panels.

The fan consists of a brushless motor directly driving a propeller. The chosen components are a T-Motor MT2814 brushless motor with an APC 12" \times 3.8 propeller. The motor is controlled by a Lynxmotion 30A Electronic Speed Controller (ESC) powered by a 5V battery eliminator circuit which is also used to power the command circuit. The ESC is controlled using a pulse width modulated signal from the Arduino microcontroller. The fan is located at the diffuser outlet where the motor is screwed onto a support cut out from doubled 3mm wood. A grid (screen) covers the outlet to protect users.

The test chamber section is square with width $a = 25$ cm and the airflow velocity is taken to be $V_a = 10$ m.s⁻¹. According to Barlow *et al* [14], the test chamber length should be between 0.5 and 3 times the hydraulic diameter, D_h , where $D_h = 2a/\pi$ [15, 13] which gives $D_h = 0.28$ m. Hence the test chamber length is chosen as $1.5D_h = 0.42$ m.

The aim of the nozzle is to concentrate and accelerate the airflow following Venturi's Law. The nozzle inlet section should be as large as possible to reduce the losses [13]; the outlet/inlet cross-section area ratio should be between 6 and 10 [15, 16]. A ratio of 6 gives a nozzle inlet width of 0.62 m. The ratio of nozzle length to width should lie between 0.667 and 1.79 for a compromise between boundary layer thickness and airflow detachment at the nozzle outlet [15]. The nozzle length is chosen as 0.55 m.

The fan/test chamber section cross-sectional area ratio ideally should lie between 2 and 3 [15, 16], but to limit the overall length of the tunnel, a ratio of 1.17 is chosen, and with a cone expansion angle of 6° [15, 16] this gives a diffuser length of 55 cm. The total length of the wind tunnel is 1.52 m.

A 2D CFD analysis using ANSYS Fluent is performed to validate the design. The geometry is divided into several sections to better control the mesh. The geometry is shown in Figure 3. The aerofoil is included with an angle of attack of 10°; the aerofoil geometry details are given in the next section. The turbulence is modelled with a $k-\omega$ Transition SST model. The simulation settings are pressure-based, steady 2D analysis with no gravity and the energy equation on. Details of the method can be found in the manual [17] (p. 4-42).

The standard $k-\omega$ model in ANSYS Fluent is based on the Wilcox $k-\omega$ model, which incorporates modifications for Low-Reynolds number effects, compressibility, and shear flow spreading. The standard $k-\omega$ model is an empirical model based on model transport equations for the turbulence kinetic energy (k) and the specific dissipation rate (ω). The model is suitable for this kind of analysis because it can be very accurate especially for the boundary-layer transition. This is a key point of the aerodynamic model developed later. The transition SST model is able to resolve the flow behaviour near a wall especially the viscous sub-layer. The model has a near-wall model approach, hence a fine mesh is needed close to the wall [17]. A representation of the mesh near to the wall is shown in Figure 4. The final mesh has 276 255 elements and 277 727 nodes; further details of the CFD meshing process are available [18].

Details of the boundary conditions and the termination criteria are given by Duran [18]. Figure 5 shows the velocity distribution results. It can be seen that there is no reverse flow inside the wind tunnel and the velocity is uniform at the inlet of the test chamber. However, the low clearance between the aerofoil and the top creates an overpressure above the aerofoil. Figures 6 and 7 show the streamlines and pressure distribution around the aerofoil respectively. The airflow around the aerofoil is not perturbed and the boundary transition location is clearly visible a few millimetres downstream of the front edge of the aerofoil. The airflow velocity profile at the wall-normal plane 70 mm downstream of the start of the test chamber section is shown in Figure

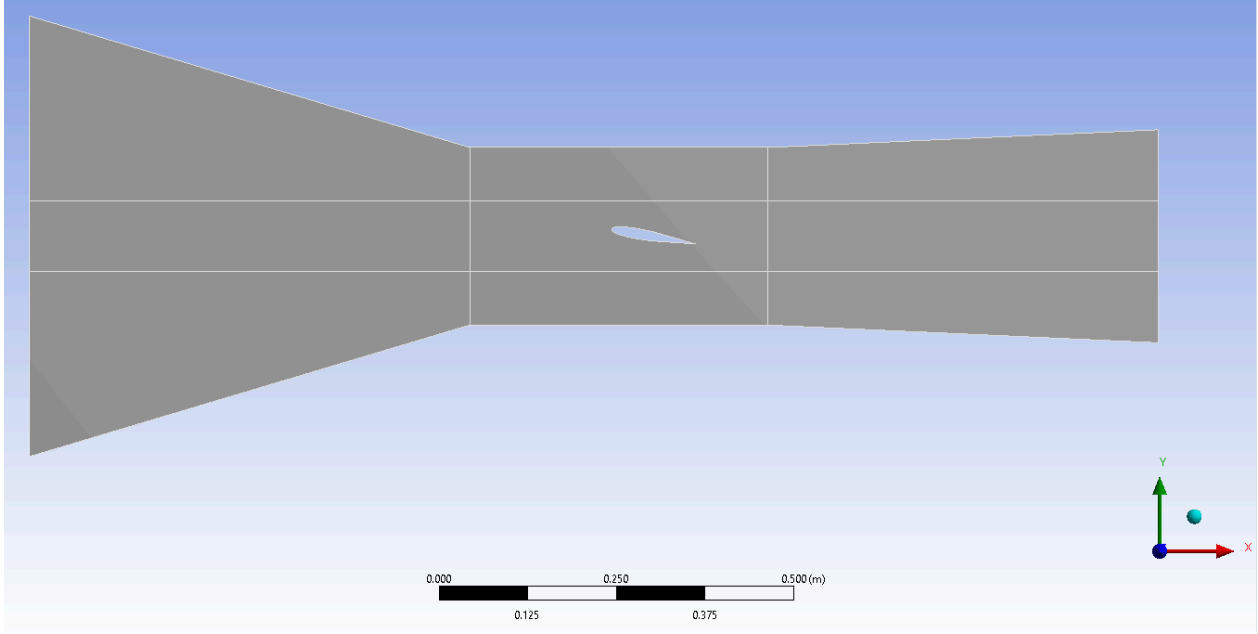


Figure 3: Geometry for CFD analysis.

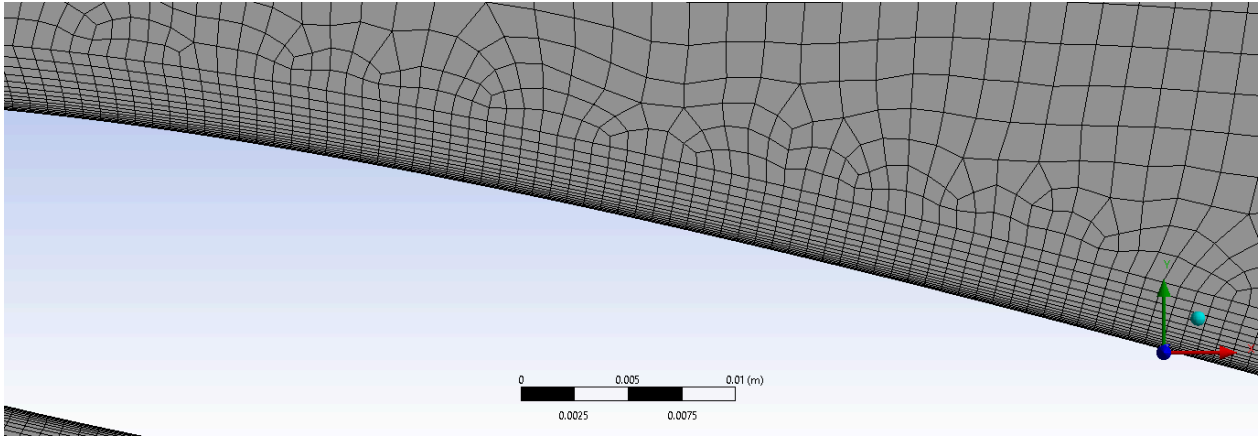


Figure 4: Mesh near to the aerofoil.

8. The average airflow velocity is $V_a = 10.15 \text{ m.s}^{-1}$ which validates the nominal design velocity of $V_a = 10 \text{ m.s}^{-1}$ used in designing the tunnel geometry. The aerofoil lift coefficient result is $C_l = 1.11$ for $\alpha = 10^\circ$.

3 Wing design and properties

In this section, the wing design is outlined, the wing aerofoil aerodynamic properties are assessed, and a dynamic model of the system is proposed. The wing is shown in Figure 9.

The aerofoil is a NACA0012, thus has zero camber with a maximum thickness of 12% of the chord, c . The control surface (elevator) pivot is located at the 80% chord point as shown in Figure 10. The deflection angle, δ , is controlled by a micro-servomotor; the linkage from the servomotor to the elevator can be seen in Figure 9. The main section is free to pivot about a point located 10 mm from the leading edge resulting in a variable angle of attack given by α . The resulting geometry is shown in Figure 10 with $\varepsilon_1 = 0.084$ and $\varepsilon_2 = 0.2$. The wing assembly centre of gravity, CG, is at the pivot point and the aerodynamic centre, AC,

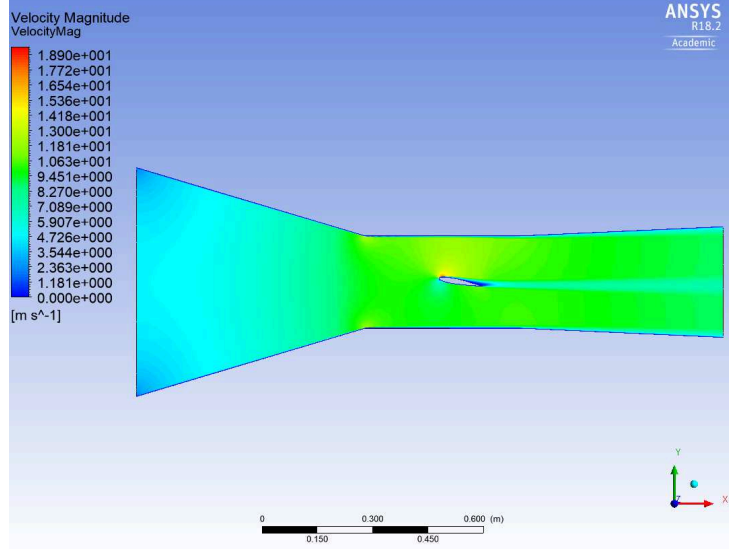


Figure 5: Velocity distribution inside tunnel.

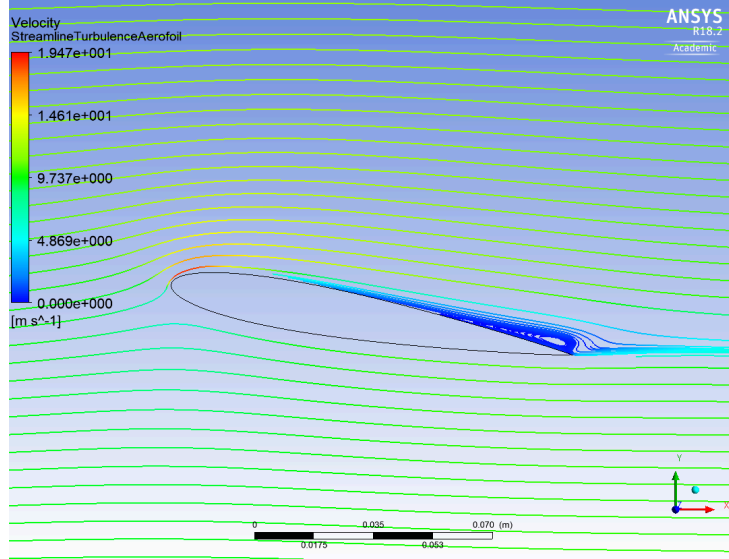


Figure 6: Streamlines around the aerofoil.

lies a distance ℓ_0 from the pivot point. The aerofoil profile is given by

$$z_t = 5t \left[0.2969\sqrt{x/c} - 0.1260x/c - 0.3516(x/c)^2 + 0.2843(x/c)^3 - 0.1015(x/c)^4 \right] \quad (1)$$

where $t = 0.12$ is the maximum thickness fraction of the chord length of the profile and z_t is the half-thickness of the profile at $x \in [0, c]$.

A CAD model of the aerofoil was created using CATIA and then 3-d printed; a visualization is shown in Figure 11. The wing was printed in two parts. There is a housing for the servomotor in the main section, with a cover that can be seen in Figures 9 and 11. The span is $s = 240$ mm and chord is $c = 119$ mm. The added crank shown is to counter-balance the wing so that the wing assembly centre of gravity, CG, is at the pivot point. The crank is made from 3mm wood sheet and the pivot shaft is 6mm aluminium tube; the servomotor wiring runs inside the tube. The wing is hollow and is hence quite light. The moment of inertia of the wing is calculated from the CAD model by CATIA to be $I = 1544$ kg.mm².

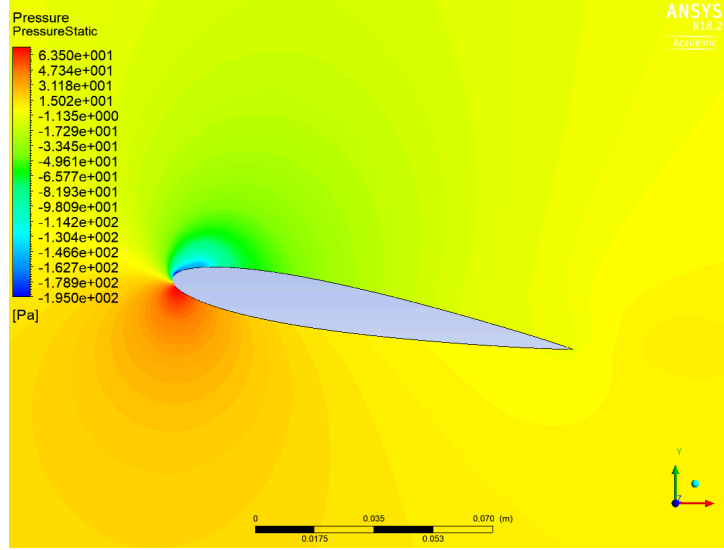


Figure 7: Pressure distribution around the aerofoil.

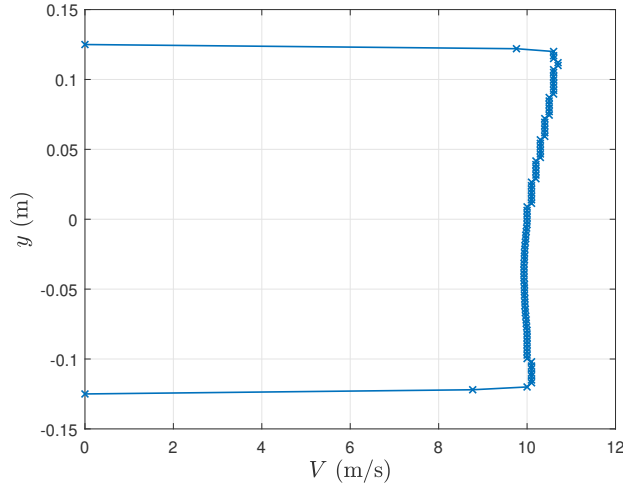


Figure 8: Airflow velocity profile upstream of the aerofoil.

The lift coefficient, C_l , at the aerodynamic centre is given by

$$C_l = a_{1v}\alpha + a_{2v}\delta \quad (2)$$

where α is the angle of attack, a_{1v} is the viscous lift-curve slope of the aerofoil and a_{2v} is the lift-curve slope with respect to control surface deflection, δ . The viscous lift-curve slope is determined using ESDU 97020 [19] and ESDU 72024 [12] as $a_{1v} = 0.11(^{\circ})^{-1}$. This has been validated using JavaFoil [18]. The control surface characteristic is determined from ESDU C010103 [20] as $a_{2v} = 0.058(^{\circ})^{-1}$ and is valid for $\delta \in [-15^{\circ}, 15^{\circ}]$. Details of the calculations are in the Appendix.

The moment curve slope with respect to control surface deflection, m_0 , at the aerodynamic centre is evaluated using ESDU C080101 [21] as $m_0 = 0.01(^{\circ})^{-1}$. Details of the calculations are also in the Appendix.

4 Instrumentation, controller and GUI

The control algorithms are implemented via an Arduino Nano with an ATmega328 microcontroller. The pitch angle is assumed to equal to the angle of attack and is measured with a 10 k Ω rotational potentiometer

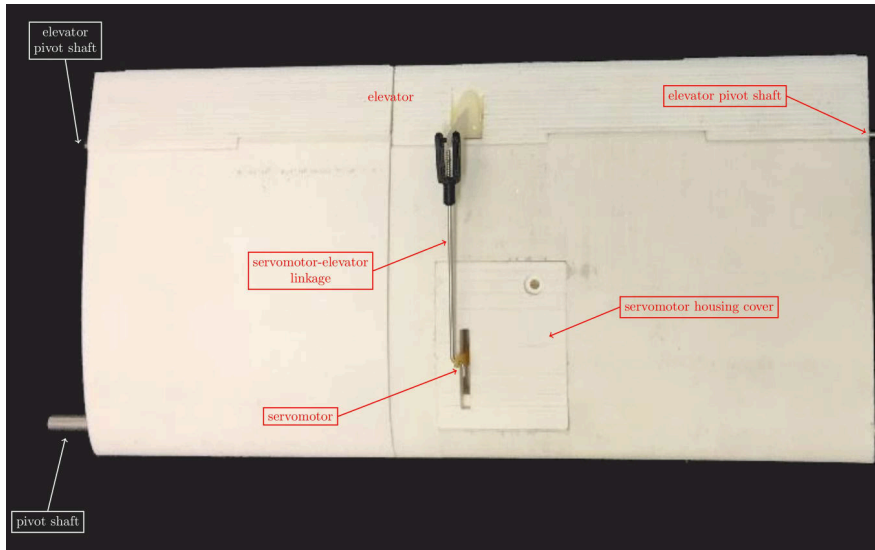


Figure 9: Wing with servomotor-elevator linkage.

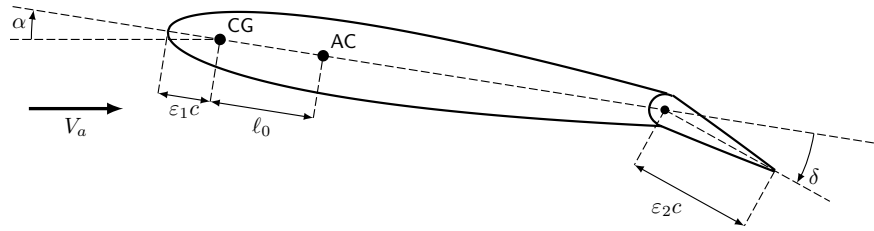


Figure 10: Aerofoil.

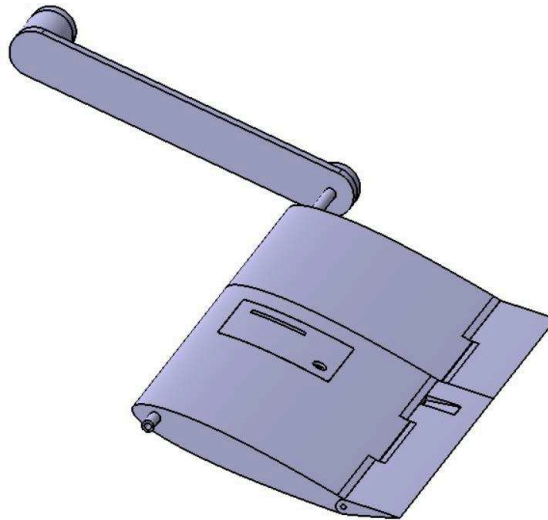


Figure 11: Wing assembly CAD Model.

attached to the shaft with a flexible coupler. A Bluetooth HC-05 module is included to communicate with the laptop PC.

The microcontroller is programmed in C++ using the Arduino IDE. The code is constituted by two loops, i) the control loop running at 2ms including the PID control and ii) the communication loop running at 25ms.

The PID control is implemented in a standard parallel form as

$$u(t_k) = k_p e(t_k) + k_i \Delta t \sum_{i=1}^k e(t_i) + k_d / \Delta t (e(t_k) - e(t_{k-1})) \quad (3)$$

where $u(t_k)$ is the control signal at k th sample time, t_k ; $\Delta t = t_k - t_{k-1}$ is the sample period which is constant, and (k_p, k_i, k_d) is the triplet of PID control gains. Windup protection is implemented using simple clamping. The potentiometer signal is pre-filtered to reduce noise. The data is buffered and communicated to the GUI in the communication loop. Details of the circuit and code are available in Duran [18].

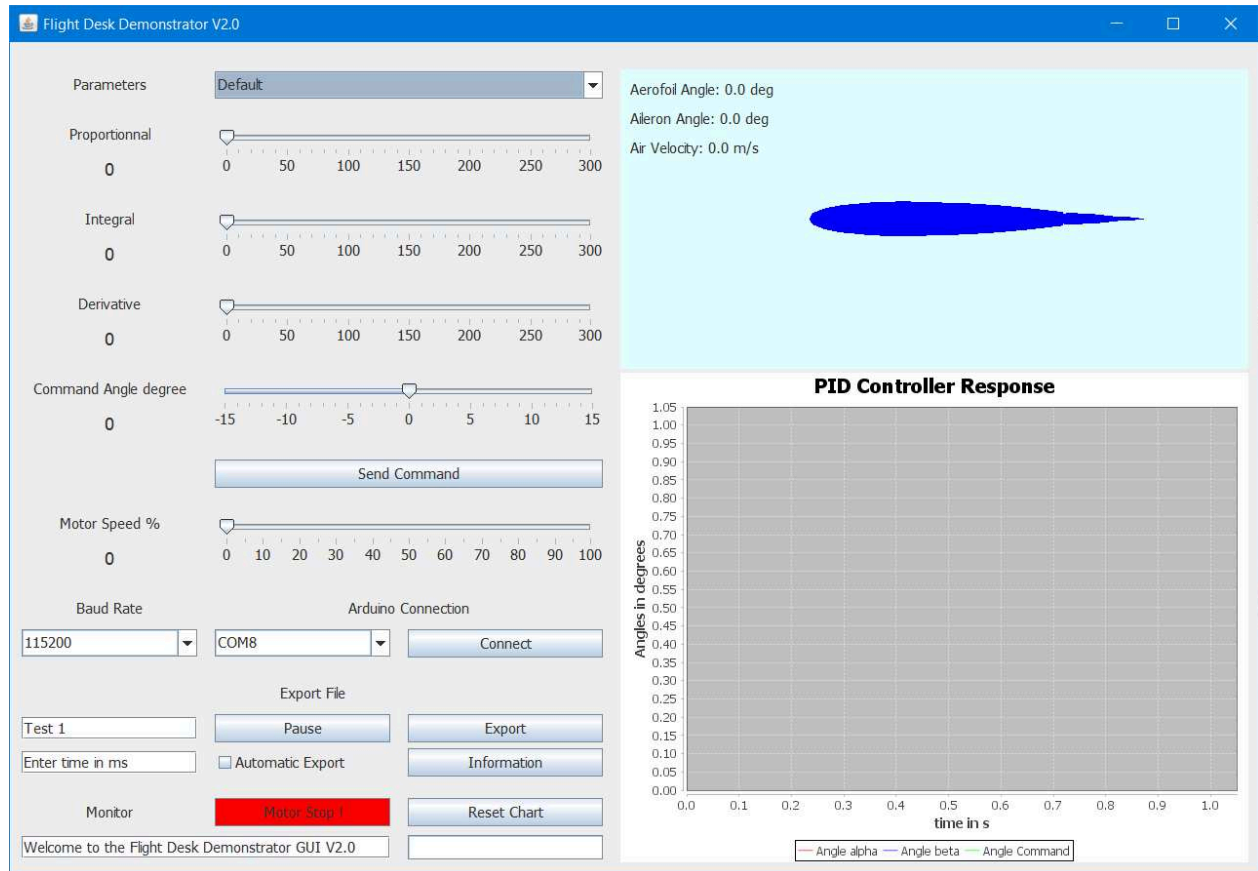


Figure 12: Graphical user interface screenshot.

The GUI provides five main features:

- A real time animation driven by the data measured from the board.
- A chart displaying the command angle, α_d , the angle of attack of the aerofoil, α , and the winglet control angle, δ .
- A control panel for setting the PID gains, the motor speed and the command angle.
- An Arduino connection panel for choosing the right COM port and the right BAUD rate.
- A monitor panel with facilities to export the data and reset the chart, an ‘information’ button for help and a red stop button for switching off the fan motor. There is also a ‘progress’ bar and a text bar to give some information to the user.

A screenshot of the GUI is shown in Figure 12. The GUI is programmed in Java using the Eclipse IDE. The GUI can be connected to the Arduino using either a USB port or a Bluetooth connection. Both are serial communication protocols. It is possible to select the Baud rate and the right COM port.

The codes for both the Arduino and the GUI are available [22]¹.

5 System model and results

From Figure 10, the pitch angle response can be modelled by the ordinary differential equation

$$I\ddot{\alpha}(t) = -qS\ell_0a_{1v}\alpha(t) + qS(\ell_0a_{2v} + cm_0)\delta(t) - b\dot{\alpha}(t) \quad (4)$$

where I is the moment of inertia of the aerofoil assembly about the shaft, b is a friction and aerodynamic damping coefficient that is assumed to be constant, $S = sc$ is the wing area and $q = 1/2\rho V_a^2$ where ρ is the air density. The remaining coefficients are defined in the Aerofoil design and properties section. If the servomotor dynamics are approximated with a first order lag with time constant T , then taking Laplace transforms, the dynamics can be represented by the generic third order system transfer function, $G(s)$, where

$$G(s) = \frac{k_g}{(s^2/\omega_n^2 + 2\zeta s/\omega_n + 1)(Ts + 1)} \quad (5)$$

where k_g is the steady state gain, ζ is the damping ratio and ω_n is the natural frequency of the dominant mode. The damping ratio is mostly dependent on the friction and some aerodynamic damping, both of which are small, hence $\zeta < 1$ and the dominant mode poles are complex.

The open-loop response with the fan-motor speed set to 65% is displayed in Figure 13. This shows that the response is dominated by an underdamped mode. There is also significant disturbance to the wing angle, this is possibly a result of unsteady air-flow in the wind tunnel resulting from vortex shedding off the corners between the nozzle and test chamber sections.

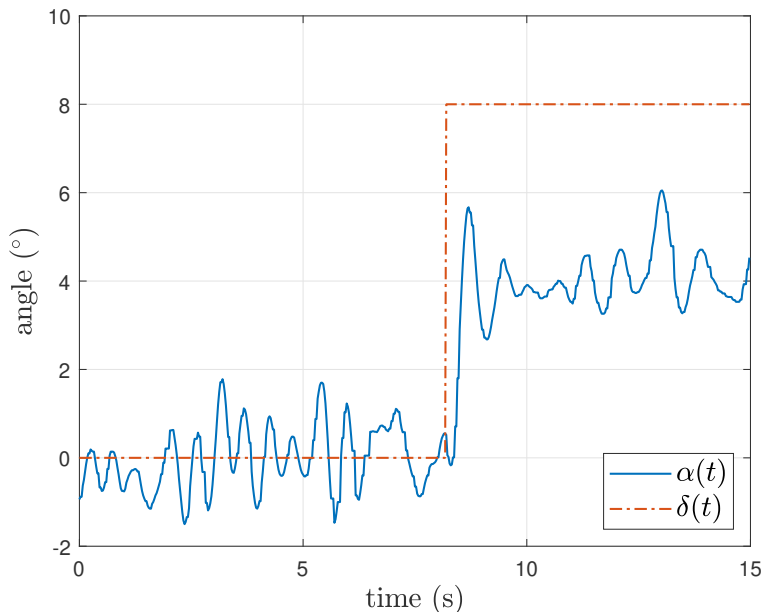


Figure 13: System open-loop response to change in elevator angle.

Using the GUI interface, various controller gains can be applied. If proportional negative feedback is applied with a gain of $k_p = 0.67$ and the fan-motor speed set to 65%, the wing starts to oscillate with a period of 0.58 s. This confirms that the damping ratio is low and the presence of servo lag inside the operational bandwidth. Figure 14 shows the step response with proportional control with the gain reduced

¹Also available on GitHub (<https://github.com/JojoLico/Flight-Desk-Control-Demonstrator>)

by half, that is $k_p = 0.34$, which gives a stability gain margin of 6 dB. The low loop gain means that there is large steady state error and poor disturbance rejection properties as can be seen from the response.

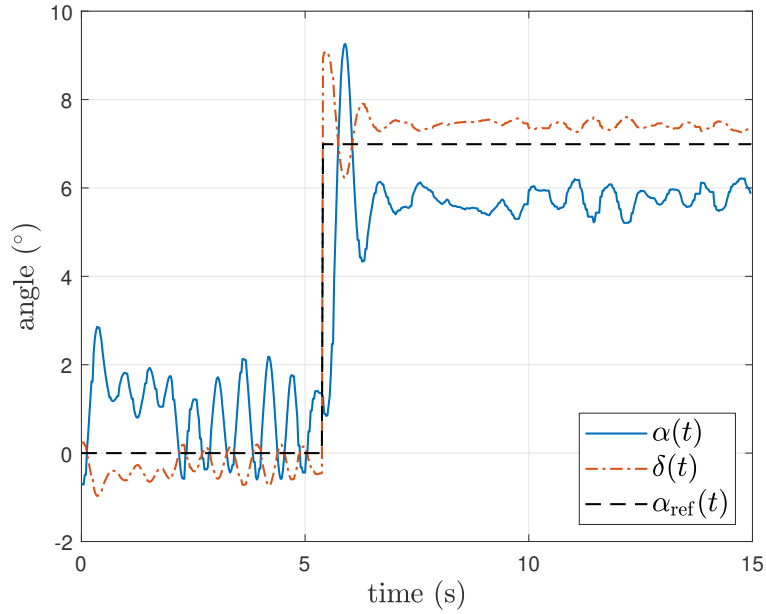


Figure 14: System response with a proportional controller.

Derivative action is introduced to improve the stability and increase the damping. Integral action is included to eliminate steady state error and improve the low frequency disturbance rejection. The GUI allows easy empirical tuning of the gains. For example, with the fan-motor speed set to 65% and $k_p = 0.1$, $k_i = 2.5$, $k_d = 0.2$, the step response to a pitch angle reference, α_{ref} , demand change from 0° to 7° results in the response shown in Figure 15. The response is fast with about 20% overshoot. The steady state error is eliminated and the disturbance effects reduced.

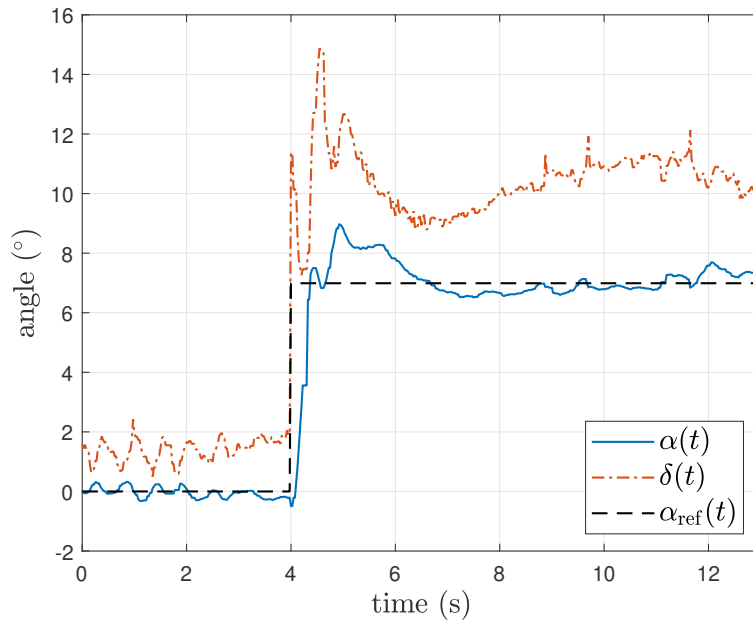


Figure 15: System response with a PID controller tuned empirically.

6 Conclusions

The paper describes the design of a benchtop wind tunnel and wing pitch control mechanism suitable for demonstration and laboratory experiments for aerospace students on a first course in control systems. The equipment was constructed at a relatively low-cost. It performs well to demonstrate the principles of basic feedback control within a context of fixed-wing aerodynamics. This means the relevance of feedback control to flight control and servo position control can be made less abstract for aerospace and aeronautic students. The GUI allows rapid and easy variation of the control gains, and the effects of standard 3-term PID control can be demonstrated to students.

The CFD analysis of the tunnel provides a prediction of that the quality of the flow and that the mean airspeed are suitable for the experiment. A high quality of flow is not required since the purpose of the tunnel is to enable the control system experiment, not to obtain accurate analysis of the fluid flows. In practice, control systems are subject to disturbances, and the flow disturbances that are evident from the results are helpful in showing to students the ability of feedback control to attenuate the effect of disturbances on the output. However, the analysis is only for a two dimensional model of the CFD, so three-dimensional wall effects are not considered. A fuller three-dimensional model and flow validation remains for further work that is suitable for student project work.

The aerodynamic coefficients were calculated using ESDU Aerodynamic Series, and validated using JavaFoil. Experimental validation remains for further work that would be suitable for student projects.

At present, the modelling of the system is incomplete. Measurements of the aerofoil assembly moment of inertia have not been made. A trim map could be easily constructed by experiment and the plant gain obtained. Experimental determination of the natural frequency, the damping ratio and the servomotor time constant also remain for further work that is also suitable for student projects. A full model will allow control analysis, design and simulation of the system that could be incorporated into a control system course.

The equipment could also be used by students for control design project work, for example to design robust, gain-scheduling or adaptive controllers. In addition, by appropriate choice of feedback gain, the system demonstrates instability in the form of a limit-cycle; thus some non-linear effects can be demonstrated.

Appendix — ESDU Wing Characteristics Calculations

Some details of the lift characteristic calculations using ESDU Aerodynamics Series [19, 12, 20, 21] are presented below. The notation is largely as for the ESDU sources where further details of the calculation procedures can be found. Additional details are in Duran [18].

Firstly, the inviscid lift-curve slope, a_{1i} , is calculated [12]. The trailing edge angle, τ , is calculated from $\tau = 2 \arctan(-dz_t/dx)$ evaluated from Eq. (1) at $x/c = 1.0$ as $\tau = 16^\circ$. The parameter z_{t2} is determined from Eq. (1) for $x/c = 0.05$ giving $2z_{t2}/t = 0.59$. The coefficient $F_1 = 0.819$ is read from Figure 1 of ESDU 72024 [12] giving the inviscid lift-curve slope calculated from $a_{1i} = 0.10967(1 + F_1 t/c) = 0.1204$.

The aerodynamic centre is determined from the coefficient F_3 from Figure 4 of ESDU 72024 [12]. The parameter $x_t/c = 0.3$ is determined from Eq. (1) where x_t/c is the chord fraction where the thickness is maximum, that is where $dz_x/dx = 0$. The parameter z_{t1} is determined from Eq. (1) for $x/c = 0.005$ giving $2z_{t1}/t = 0.2$. The aerodynamic centre is given by $x_{ai} = (1 + F_3 t/c)/4$ where $F_3 = 0.275$.

The viscous lift-curve slope is calculated using ESDU 97020 [19]. The trailing edge parameter, τ_a , is determined from

$$\tan(\tau_a/2) = \frac{t_{0.9} - t_{0.99}}{0.18c} \quad (6)$$

where $t_{0.9}$ and $t_{0.99}$ are respectively the aerofoil thickness at $x/c = 0.9$ and $x/c = 0.99$. From Eq. (1), $\tan(\tau_a/2) = 0.134$. For the nominal flow speed of $V_a = 10 \text{ m}\cdot\text{s}^{-1}$ and a kinematic viscosity for atmosphere at sea level given by $\nu = 0.146 \times 10^{-6} \text{ m}^2\cdot\text{s}^{-1}$, the Reynolds number is $R_N = V_a c/\nu = 82.2 \times 10^3$.

The boundary layer transition location varies rapidly with angle-of-attack [23]. Here we assume that transition occurs at mid-chord and the flow is incompressible, then extrapolating from Figure 6 of ESDU 97020 [19] gives the lift-curve slope reduction factor of 0.91 resulting in a viscous lift-curve slope $a_{1v} = 0.11(^{\circ})^{-1}$. Note that $R_N = 82.2 \times 10^3$ is a fairly low value, and is outside the range validated for ESDU 97020 [19]. Low Reynolds number aerodynamic characteristics of a NACA 0012 aerofoil are considered by Kim *et al* [24],

and their review indicates that nonlinear effects are not too significant for Reynolds numbers above 50×10^3 . Hence this value is assumed to be reasonably accurate.

The control surface characteristic is determined from ESDU C010103 [20]. The lift coefficient, C_l , at the aerodynamic centre is given by Eq. (2). The inviscid lift-curve slope, a_{2T} , is determined using Figure 1 from ESDU C010103 [20] with $\varepsilon_2 = 0.2$ and with $t/c = 0.12$ giving $a_{2T} = 3.65 \text{ rad}^{-1}$. Using the lift-curve slope reduction factor of 0.91 determined earlier, $a_{2v} = 0.058(^{\circ})^{-1}$.

In a similar fashion, the moment-curve slope with respect to control surface deflection, m_0 , at the aerodynamic centre is evaluated using ESDU C080101 [21]. From Figure 1 of ESDU C080101 [21], the inviscid flow moment-curve slope is $m_{0T} = 0.64 \text{ rad}^{-1}$, and from Figure 2 of ESDU C080101 [21] the reduction factor is 0.90 giving $m_0 = 0.01(^{\circ})^{-1}$.

References

- [1] Kheir NA, Åström KJ, Auslander D, Cheok, KC, Franklin GF, Masten M and Rabins M. Control systems engineering education. *Automatica* 1996; 32(2): 147–166. DOI:10.1016/0005-1098(96)85546-4.
- [2] Åström KA and Östberg AB. A teaching laboratory for process control. *IEEE Control Systems Magazine* 1986; 6(5): 37–42. DOI:10.1109/MCS.1986.1105142.
- [3] Wellstead PE. Teaching control with laboratory scale models. *IEEE Transactions on Education* 1990; 33(3): 285–290. DOI:10.1109/13.57074.
- [4] Dorf RC and Bishop RH. *Modern Control Systems*. 11 ed. Upper Saddle River, NJ: Pearson Prentice Hall, 2008.
- [5] National Instruments/QUANSER. QNET 2.0 vertical take-off and landing board for NI ELVIS. Product information sheet. URL <https://www.quanser.com/products/qnet-2-0-vtol-board/>.
- [6] Feedback Instruments. Twin rotor MIMO. url, 2018. URL <https://www.leybold-shop.co.uk/ve6-3-5-12.html>.
- [7] Apkarian J, Lévis M and Fulford C. *Laboratory Guide: 2 DOF Helicopter Experiment for LabVIEW Users*. QUANSER, 2012. QUANSER.
- [8] Apkarian J, Lévis M and Fulford C. *Laboratory Guide: 3 DOF Helicopter Experiment for LabVIEW Users*. QUANSER, 2012. QUANSER.
- [9] Apkarian J and Lévis M. *Laboratory Guide: 3 DOF Hover Experiment for LabVIEW Users*. QUANSER, 2013. QUANSER.
- [10] QUANSER. Autonomous Vehicles Research Studio. Product information sheet, 2018. URL <https://www.quanser.com/products/autonomous-vehicles-research-studio/>.
- [11] Tecquipment Academia. AF41 — Flight Demonstration Wind Tunnel. Datasheet. URL <https://www.tecquipment.com/flight-demonstration-wind-tunnel>.
- [12] ESDU 72024. Aerodynamic characteristics of aerofoils in compressible inviscid airflow at subcritical Mach numbers. ESDU Aerodynamics Series 72024, ESDU, 1999.
- [13] Mauro S, Brusca S, Lanzafame R, Famoso F, Galvagno A, and Messina M. Small-scale open-circuit wind tunnel: Design criteria, construction and calibration. *International Journal of Applied Engineering Research* 2017; 12(23): 13649–13662.
- [14] Barlow JB, Rae WH Jr and Pope A. *Low Speed Wind Tunnel Testing*. New York: Wiley-Interscience, 1999.
- [15] Brusca S, Lanzafame R and Messina M. Low-speed wind tunnel: Design and build. In Pereira JD (ed.) *Wind Tunnels: Aerodynamics, Models and Experiments*. Nova Press, 2011. pp. 189–220.

- [16] Bell JH and Metha RD. Contraction design for small low-speed wind tunnels. Technical Report JIAA TR-84, JIAA, Technical Report, 1988.
- [17] ANSYS. ANSYS FLUENT 12.0: Theory Guide. Manual, 2009.
- [18] Duran JR. *Flight Desk Control Demonstrator*. MSc dissertation, Cranfield University, Bedfordshire, U.K., 2018. DOI:10.17862/cranfield.rd.8052650.
- [19] ESDU 97020. Slope of aerofoil lift curve for subsonic two-dimensional flow. ESDU Aerodynamics Series 97020, ESDU, 1997.
- [20] ESDU C010103. Rate of change of lift coefficient with control deflection in incompressible two-dimensional flow, $(a_2)_0$. ESDU Aerodynamics Series AERO C.01.01.03, ESDU, 1978.
- [21] ESDU C080101. Rate of change of pitching moment coefficient with control deflection for a plain control in incompressible two-dimensional flow, m_0 . ESDU Aerodynamics Series AERO C.08.01.01, ESDU, 1956.
- [22] Duran JR, Whidborne JF, Carrizales Rodriguez M and Pontillo A. A benchtop flight control demonstrator — data and code. Cranfield Online Research Data (CORD) repository, 2019. DOI: 10.17862/cranfield.rd.8052650.
- [23] Yousefi K and Razeghi A. Determination of the critical Reynolds number for flow over symmetric NACA airfoils. In *AIAA SciTech Forum*. AIAA 2018-0818. DOI:10.2514/6.2018-0818.
- [24] Kim DH, Chang JW and Chung J. Low-Reynolds-number effect on aerodynamic characteristics of a NACA 0012 airfoil. *Journal of Aircraft* 2011; 48(4): 1212–1215. DOI:10.2514/1.C031223.